NEUTRON TRANSMISSION MEASUREMENTS AND RESONANCE ANALYSIS OF MOLYBDENUM-96

J.M. Brown, A. Youmans, N. Thompson, and Y. Danon
Gaerttner LINAC Center
Mechanical, Aerospace, and Nuclear Engineering Department
Rensselaer Polytechnic Institute
110 8th St, Troy, NY 12180
brownj25@rpi.edu; danony@rpi.edu

D.P. Barry, G. Leinweber, M.J. Rapp, R.C. Block
Bechtel Marine Propulsion Corporation
P.O. Box 1072, Schenectady, NY 12301-1072

Rian Bahran
Los Alamos National Laboratory
Los Alamos, NM

ABSTRACT

Isotopes of molybdenum can be found as high yield fission products in nuclear power reactors, certain alloys of steel used in nuclear reactors, and proposed U-Mo nuclear fuels [1]. As computational power and accuracy rapidly increase, nuclear data becomes a greater fraction of the uncertainty in neutron transport calculations. This work is part of an effort to increase the accuracy of existing total cross section evaluations to improve the accuracy of computational simulations. Neutron transmission measurements were performed at the Rensselaer Polytechnic Institute Gaerttner Linear Accelerator Center using the time-of-flight method with a metallic enriched ^{96}Mo sample from 113 eV to 20 keV. In addition a method was developed to process data and to ensure the accuracy of the flight path length and neutron emission time using depleted uranium to validate resonance energies. Measurements in the mid-low energy region (113 eV – 4.8 keV) were performed at a 32 m flight path distance with a ^{6}Li glass scintillation detector, and measurements in the mid-high energy region (4.5 keV – 20 keV) were performed at 100 m with an array of ^{6}Li glass scintillation detectors. Using the R-matrix Bayesian fitting code SAMMY 8.0, previously identified resonances have been modified to appropriate spin groups, neutron widths, and energies. The s-wave strength function was found to be $S_0 = 0.82 \pm 0.32$, and the capture resonance integral RI_γ is in agreement with the ENDF/B-VII.1 calculated value. These results agree with the values published in the Atlas of Neutron Resonances by Brookhaven National Laboratory.

KEYWORDS
Molybdenum, transmission, resonance parameters, total cross-section, RPI

1. INTRODUCTION

As computer power and modeling accuracy quickly increase, an increasing fraction of uncertainty in neutron transport codes and reactor calculations is contributed by nuclear data libraries. In an effort to increase the accuracy of existing nuclear data libraries, neutron transmission measurements were performed at the Rensselaer Polytechnic Institute Gaerttner Linear Accelerator Center (LINAC), using the time-of-flight method with a metallic ^{96}Mo sample of enrichment 96.8 ± 0.1% and thickness 0.0547 ± 0.0001 atoms/barn [2]. Transmission measurements were performed at both 32 and 100 m to ensure accuracy over a large energy range of resonances.

2. EXPERIMENTAL CONDITIONS

The Gaerttner Linear Accelerator Center at Rensselaer Polytechnic Institute (RPI) houses an electron linear accelerator which operates by pulsing electrons, accelerating them by microwave radiation to energies of ~55 MeV, and directing them towards a water-cooled tantalum target. The electrons interact with the tantalum atoms producing Bremsstrahlung radiation which induces a nuclear (γ,n) reaction in the tantalum plates, thus emitting neutrons [3]. Neutrons are produced in a wide range of energies as high as 60 MeV, which is referred to as a "white" neutron source. Many of these neutrons interact with water molecules in the target, softening the neutron energy spectrum.

The initial time of neutron production is referred to as t_0, and is important for determining the energies of neutrons interacting with the detector. Highly energetic neutrons have a greater velocity than lower energy neutrons and therefore require less time to travel the distance from the neutron producing target to the detector. This distance is referred to as the flight path (FP). The time energy relationship is given by Eq. 1, where t_i is the time at which a neutron was recorded in time bin i as having interacted with the detector, E_i is the corresponding kinetic energy of the neutron, and k is a proportionality constant. Eq. 1 assumes the neutron is traveling at non-relativistic speeds, which is relevant to the energy range of the experiment described here.

$$E_i = \left(\frac{k * FP}{t_i - t_0}\right)^2 \tag{1}$$

At the 100 m flight station a Mid-Energy ^{6}Li-glass Neutron Detector Array (MELINDA) [1] was used to detect neutron interactions. The MELINDA detector is an array of four 1.27 cm thick ^{6}Li glass detectors each in a low-mass, light-tight aluminum casing coupled to two 12.7 cm diameter out-of-beam photomultiplier tubes; it was described in more detail in Ref. 2. At 32 m a similar 1.27 cm thick ^{6}Li glass detector is optically coupled to two out-of-beam photomultiplier tubes. ^{6}Li glass detectors activated with Ce are widely used as neutron detectors due to their fast timing characteristics [1,4] and high (n,alpha) neutron cross section. Lower energy measurements (0.113-4.8 keV) were taken at the 32 m FP and higher energy measurements (4.8-20 keV) were taken at the 100 m FP in order to optimize counting statistics and experimental energy resolution. The electronic data acquisition system was described in detail in Ref. 3. The LINAC was operated at 400 pulses per second, with a pulse width of ~12 ns.

Samples were placed on a rotating sample changer; this included ^{96}Mo, depleted uranium, and an open position used for the transmission calculation. The metallic 0.878 cm thick (0.5654 atoms/b) ^{96}Mo sample was obtained from the National Isotope Center at Oak Ridge National Laboratory (ORNL) with an isotopic enrichment of 96.8% (atomic percent), as well as approximately 0.2% ^{92}Mo, 0.2% ^{94}Mo, 0.9% ^{95}Mo, 1% ^{97}Mo, 0.8% ^{98}Mo, and 0.2% ^{100}Mo. A 1.587 cm thick depleted uranium sample was used to verify experimental quantities such as the FP, further discussed in Section 3. A fission chamber located at

a FP of ~ 9 m monitored the beam intensity, and was used to normalize any beam intensity fluctuations, as well as verify collection times for sample positions.

3. DATA REDUCTION

The data reduction process for a transmission experiment includes: dead-time correcting, summing the counts from separate runs that correspond to each sample/beam condition, monitor normalization, estimating the background, and subsequently calculating the transmission. Neutron transmission is calculated using Eq. 2,

$$T_i = \frac{C_{s,i} - k_s B_{s,i} - B0_s}{C_{o,i} - k_o B_{o,i} - B0_o} \tag{2}$$

where $C_{s,i}$, $B_{s,i}$, $B0_s$ are the dead time corrected and monitor normalized detected count rates, calculated time dependent background rate, and constant background rate corresponding to when a sample is in the neutron beam. $C_{o,i}$, $B_{o,i}$, $B0_o$ are the same quantities corresponding to when there is no sample in the neutron beam, which is referred to as the open beam. The values of k_s and k_o are normalization constants for the background. The transmission is calculated for each time bin given by the index i, which is often transformed using Eq. 1 to transmission as a function of energy. Background determination often consumes a large fraction of the analysis time for transmission data reduction, and will be discussed in Section 4. Another important quantity that must be verified is the energy of neutrons that interact with the detector. Neutron energies depend on two quantities in this context: time-of-flight (TOF), and the FP. The FP depends on where in the photoneutron target a neutron is produced and where it interacts along the thickness of the detector glass, which are sources of uncertainty. The neutron TOF depends on when the neutron is recorded as having interacted with the detector (t_i) and when the neutron was born (t_0) i.e., emitted from the Ta nucleus. The time resolution of the ^{6}Li glass is of the order of a few nanoseconds [1,5] and is recorded in bins of width 6.4 ns. The quantity t_0 was determined by locating the gamma flash, a pulse of Bremsstrahlung gammas resulting from the (e^-,γ) reaction in the Ta target that are transmitted to the detector. The gamma flash for this experiment on average had a Gaussian distribution with ~14 ns FWHM.

In order to verify the FP and t_0 the transmission of a sample of depleted uranium was measured and compared to a SAMMY 8.0 calculated function of transmission using ENDF evaluated resonance parameters; this is shown in Figure 1. This also verifies the RPI resolution function which is coded into SAMMY 8.0 [6]. The resolution function describes the convolution in time space of when neutrons are born in the tantalum target and when they interact with the lithium detector.

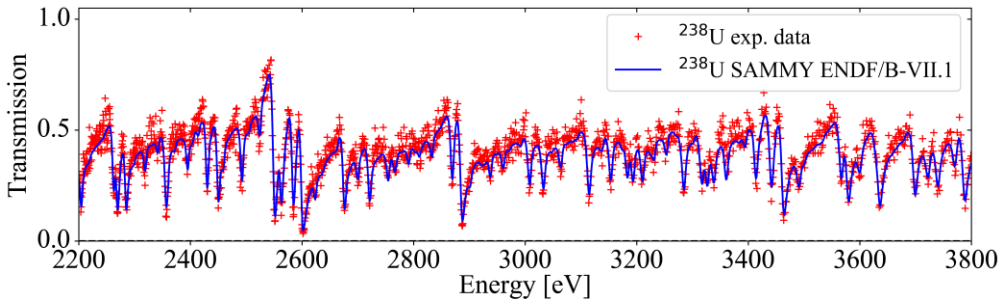

Figure 1. Transmission of depleted uranium at ~32 m and the corresponding fit from SAMMY 8.0 using ENDF/B-VII.1 resonance parameters, ensuring the flight path and time zero provide the best fit.

The SAMMY code is designed to incorporate experimental conditions to fit experimental data with the proper resonance parameters. Instead of fitting, in this case ENDF/B-VII.1 parameters are used to generate Doppler and resolution broadened transmission as a function of energy to make a comparison to experiment, operating on the assumption that ENDF values for depleted uranium are accurate. Having verified FP, t_0, and resolution function with the depleted uranium the sample of interest can be evaluated. The RPI measurement of ^{96}Mo was found to have small discrepancies with ENDF/B-VII.1 concerning resonance energies, six spin group assignments, and neutron widths. A portion of RPI data is shown in Figure 2 along with transmission calculated by the SAMMY 8.0 code using both newly fitted and ENDF/B-VII.1 resonance parameters.

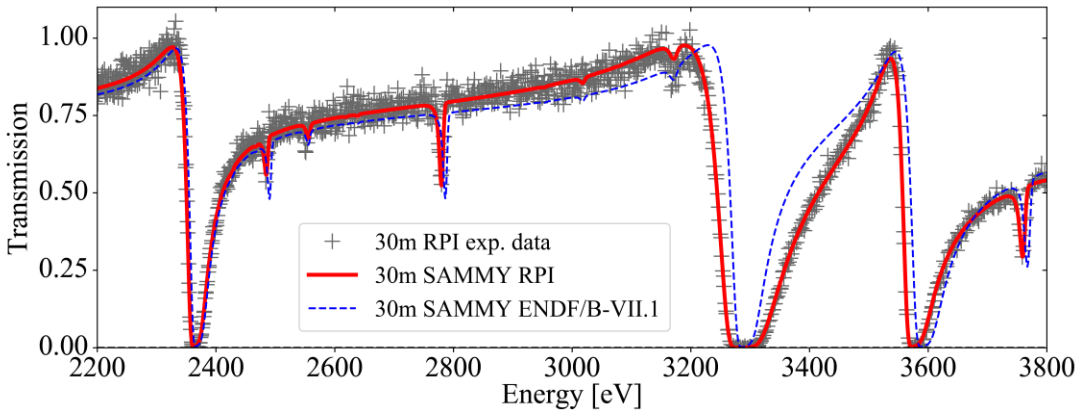

Figure 2. Transmission of ^{96}Mo and the corresponding SAMMY 8.0 fit using the newly updated resonance parameters and ENDF/B-VII.1 resonance parameters.

4. BACKGROUND ANALYSIS

In TOF experiments, and especially neutron transmission experiments, background radiation may distort the desired signal of transmitted neutrons interacting with the detector. Part of this undesired signal is due to natural background radiation from radioactive elements in the earth and cosmic radiation, which is relatively constant in time and can be measured for a given day or experiment, represented as B0 in Eq. 2. The other portion is the "in-beam" time dependent background caused by off-energy neutrons and Bremsstrahlung gamma rays, which is more difficult to disentangle. Several methods have been developed to characterize the background for transmission measurements, one of which is the method employed for this measurement: the "black notch" method. This involves placing material in the neutron beam that have resonances with large cross sections at specific neutron energies. This allows the experimentalist to remove all the neutrons in the beam at that energy, leaving only the off-energy neutrons and gamma rays to interact with the detector. This is done with several different materials during an experiment, each having resonances at a different energies. An example of a "black notch" is shown in Figure 3; a notch is considered black if the counts as a function of time are somewhat constant, such as the region that has been highlighted in Figure 3. The count rate is determined for each black notch with each sample configuration and a background function is fitted to the background points calculated. This can be seen in Figure 4, where the notches are obtained from Na, Mn, Co, and W.

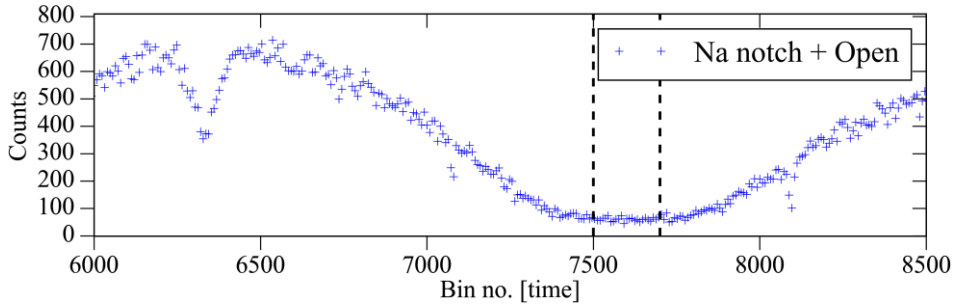

Figure 3. Shown above are counts as a function of time, given in grouped bins. Na notch is in the beam, with Open sample position. Delineated is the flat "black" region chosen to calculate the counts per second of the Na notch used in background analysis.

To properly compare notches we calculate the counts per second found at the resonance energy using Eq. 3 where $ch1$ and $ch2$ are the channels specifying the integration region of time bins, $counts_i$ is the counts for a given bin, b_w is the bin width (6.4 ns), and $trig$ is the number of triggers recorded by the monitor (a fission chamber is used to monitor the number of times the LINAC is pulsed).

$$CPS_{notch} = \frac{\sum_{i=ch1}^{ch2} counts_i}{(ch2 - ch1) \cdot b_w \cdot trig} \tag{3}$$

In the fitting process, it is desirable to fit only the time dependent background count rates for the notches ($B_{s,i}$ from Eq. 2), therefore the counts per second is also calculated at the end of the "rundown". At large TOF, there is a constant background component that exists before the next pulse. This constant background is what has been defined as B0 in Eq. 2. For every notch-sample configuration a B0 was calculated, and subtracted from the corresponding CPS_{notch} points. A fitting algorithm was operated to find a function of best fit to the notch points for each sample e.g., ^{96}Mo or Open. Examples of background functions calculated for this experiment are plotted in Figure 4 along with the CPS_{notch} points.

Once background functions are obtained, they are normalized by a constant value k_s or k_o at the "fixed notch". The fixed notch is a notch that is always in the beam removing neutrons at a certain energy. For the 30 m data, cobalt is placed in the beam and has a black resonance at ~132 eV. For the 100 m data sodium is always in the beam, and has a black resonance at ~2.8 keV. The normalization constants (k_s or k_o in Eq. 2) are given by the ratio of the counts per second in the fixed notch during normal beam operation (sample or open) and the background function calculated from the notch points taken during notch filter measurements (sample or open in addition to notch material in beam).

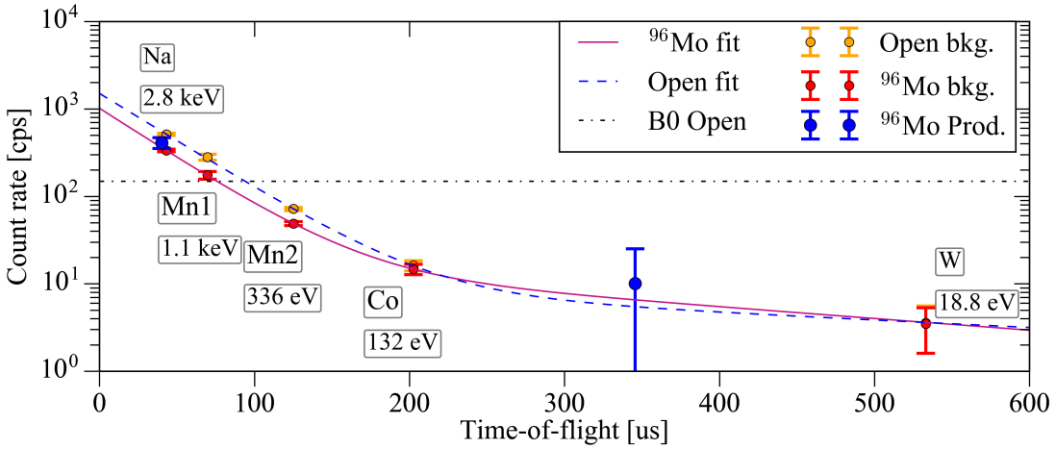

Figure 4. Time-dependent background count rates of notches and corresponding background functions are plotted as a function of time-of-flight for the open beam, and ^{96}Mo sample. Strong resonances in the ^{96}Mo sample during data production are expected to match the time-dependent count rate in the background; this is shown in blue for two resonances. An example B0 for the Open beam is shown to illustrate the background which is subtracted off.

5. RESULTS

Experimental data were fit using SAMMY 8.0 to determine resonance parameters. A total of 75 resonances for ^{96}Mo are listed in ENDF/B-VII.1. For the new fit, two resonances were removed and one resonance was added. For some resonances the total spin, parity (J^{π}), and angular momentum (l) were changed among the values already listed in order to improve the χ^2 of the fit. ENDF and new RPI parameters are listed in Table 1. Experimental uncertainties being propagated to the final parameters by SAMMY 8.0 include: counting statistics, the least squares uncertainty in the background fit, and uncertainty in the flight path and pulse width.

Table 1. ENDF and newly fitted resonance parameters are listed in order of energy for RPI parameters of each spin group. NEW highlights the space where ENDF/B-VII.1 did not contain a parameter, REMOVED highlights where an ENDF resonance was removed for the new fit. NV is listed for uncertainties when the parameter was not varied and therefore does not have an associated uncertainty. The Γ_γ values were not varied for the new fit, and the average ENDF/B-VII.1 value (136 meV) was assigned to the new resonance at 15 keV.

ENDF/B-VII.1					RPI							
J^{π}	l	E_0 [eV]	Γ_γ [meV]	Γ_n [meV]	J^{π}	l	E_0 [eV]	ΔE_0 [eV]	Γ_γ [meV]	$\Delta\Gamma_\gamma$ [meV]	Γ_n [meV]	$\Delta\Gamma_n$ [meV]
0.5	0	131.4	83	326	0.5	0	131.40	NV	83	NV	326	NV
0.5	0	2366	164	3829	0.5	0	2362.67	0.05	164	NV	4100	16
0.5	0	3287	135	8318	0.5	0	3283.3	0.1	135	NV	15670	47
0.5	0	3587	99	8000	0.5	0	3570.9	0.1	99	NV	7324	39
-0.5	1	4326	94	334	0.5	0	4318.08	0.07	94	NV	352	11
0.5	0	5385	71	4000	0.5	0	5374.99	0.09	71	NV	4536	42

0.5	0	5800	107	200	0.5	0	5787.4	0.2	107	NV	111	6
0.5	0	7909	96	3000	0.5	0	7892.9	0.1	96	NV	4994	54
0.5	0	8031	82	2000	0.5	0	8013.6	0.1	82	NV	1250	35
-1.5	1	9396	151	8000	0.5	0	9368.6	0.1	151	NV	2568	51
0.5	0	10000	120	20000	0.5	0	9978.2	0.2	120	NV	15317	107
-0.5	1	12318	136	158	0.5	0	12296.2	0.3	136	NV	810	41
0.5	0	15424	124	5000	0.5	0	15394.7	0.3	124	NV	2084	80
NEW					0.5	0	15467.9	0.3	136	NV	2418	83
0.5	0	16317	170	2700	0.5	0	16387.4	0.2	170	NV	12053	146
0.5	0	17965	114	1067	0.5	0	17923.2	0.9	114	NV	541	41
0.5	0	18107	114	1510	REMOVED							
-0.5	1	18275	136	326	0.5	0	18239.0	0.5	136	NV	1869	84
-0.5	1	19605	136	351	0.5	0	19571.6	0.4	136	NV	2821	113
0.5	0	113.4	136	0.451	-0.5	1	113.33	0.01	136	NV	0.530	0.006
0.5	0	420	136	6.06	-0.5	1	418.94	0.01	136	NV	6.12	0.09
0.5	0	969	136	2.75	-0.5	1	967.6	0.1	136	NV	3.2	0.2
-0.5	1	1269	136	2.24	-0.5	1	1265.7	0.4	136	NV	2.1	0.2
-0.5	1	1498	136	10.1	-0.5	1	1492.8	0.2	136	NV	9.6	0.5
-0.5	1	2084	136	7.5	-0.5	1	2077.1	0.4	136	NV	9.3	0.7
-0.5	1	2488	136	34	-0.5	1	2482.6	0.6	136	NV	19	2
-0.5	1	2784	136	67	-0.5	1	2777.5	0.2	136	NV	59	3
-0.5	1	3286	136	92	-0.5	1	3286	NV	136	NV	92	NV
-0.5	1	4420	136	252	-0.5	1	4411.5	0.1	136	NV	112	5
-0.5	1	4567	136	52.7	-0.5	1	4559.5	0.3	136	NV	50	3
-0.5	1	4953	136	13.7	-0.5	1	4953	NV	136	NV	13.7	NV
-0.5	1	5413	136	117	-0.5	1	5403.9	0.3	136	NV	108	7
0.5	0	7064	136	1000	-0.5	1	7051.3	0.1	136	NV	592	25
-0.5	1	7382	136	32	-0.5	1	7382	NV	136	NV	32	NV
-0.5	1	7741	136	57	-0.5	1	7725.5	0.6	136	NV	72	6
-0.5	1	7951	106	1000	-0.5	1	7934.4	0.5	106	NV	150	11
-0.5	1	8334	134	1000	-0.5	1	8316.3	0.2	134	NV	1637	52
-0.5	1	8712	136	525	-0.5	1	8695.8	0.3	136	NV	294	17
-0.5	1	10270	136	408	-0.5	1	10248.8	0.2	136	NV	1516	58
-0.5	1	10864	136	49	-0.5	1	10864	NV	136	NV	49	NV
-0.5	1	10928	136	27.7	-0.5	1	10928	NV	136	NV	27.7	NV
-0.5	1	11500	136	23.4	-0.5	1	11500	NV	136	NV	23.4	NV
-0.5	1	12051	136	292	-0.5	1	12051	NV	136	NV	292	NV
-0.5	1	13080	136	250	-0.5	1	13080	NV	136	NV	250	NV
-0.5	1	13880	136	315	-0.5	1	13855.1	0.9	136	NV	287	22
-0.5	1	14690	136	45	-0.5	1	14690	NV	136	NV	45	NV
-0.5	1	15600	136	392	REMOVED							
-0.5	1	16700	136	234	-0.5	1	16700	NV	136	NV	234	NV
-0.5	1	17245	136	35	-0.5	1	17245	NV	136	NV	35	NV
-0.5	1	19135	136	38.5	-0.5	1	19135	NV	136	NV	38.5	NV
-1.5	1	3764	80	200	-1.5	1	3755.9	0.3	80	NV	110	7
-1.5	1	5619	125	500	-1.5	1	5607.7	0.1	125	NV	275	14
-1.5	1	6046	91	1000	-1.5	1	6033.9	0.1	91	NV	265	13
-1.5	1	6570	136	1180	-1.5	1	6556.6	0.1	136	NV	315	16
-1.5	1	7776	111	200	-1.5	1	7761.7	0.2	111	NV	187	10
-1.5	1	8420	164	1000	-1.5	1	8404.4	0.1	164	NV	1363	41
-1.5	1	9090	136	985	-1.5	1	9074.5	0.2	136	NV	283	15
-1.5	1	9700	136	537	-1.5	1	9681.3	0.2	136	NV	355	18

-1.5	1	10112	160	5000	-1.5	1	10092.5	0.2	160	NV	511	30
0.5	0	11075	114	1750	-1.5	1	11051.7	0.8	114	NV	88	7
-1.5	1	11916	136	470	-1.5	1	11890.8	0.2	136	NV	1669	54
-1.5	1	13605	136	491	-1.5	1	13578.9	0.4	136	NV	528	30
-1.5	1	13944	136	275	-1.5	1	13917.2	0.4	136	NV	673	40
-1.5	1	14080	136	310	-1.5	1	14054.2	0.7	136	NV	217	16
-1.5	1	14478	136	451	-1.5	1	14450.7	0.3	136	NV	953	52
-1.5	1	15027	136	461	-1.5	1	14997.9	0.8	136	NV	248	19
-1.5	1	15351	118	5000	-1.5	1	15320.7	0.3	118	NV	2371	72
-1.5	1	15815	214	6000	-1.5	1	15782.1	0.3	214	NV	1552	67
-1.5	1	16166	136	619	-1.5	1	16133.6	0.5	136	NV	580	35
-1.5	1	16428	136	416	-1.5	1	16428	NV	136	NV	416	NV
-1.5	1	16800	136	213	-1.5	1	16788.0	0.5	136	NV	2391	129
-1.5	1	17042	136	170	-1.5	1	17009.1	1.2	136	NV	225	18
-1.5	1	17790	170	1500	-1.5	1	17756.5	0.4	170	NV	1177	66
-1.5	1	18565	136	1020	-1.5	1	18531.9	0.5	136	NV	1471	78
-1.5	1	18995	136	892	-1.5	1	18957.4	0.4	136	NV	1714	84
-1.5	1	19375	200	3800	-1.5	1	19336.1	0.4	200	NV	2712	98

Following the fitting procedure, it was desirable to quantify the effect these changes would have on the resulting capture resonance integral (RI_γ) and the strength function (S_0) derived from newly designated s-waves and neutron widths. The RI_γ was calculated from Eq. 4.

$$RI_\gamma = \int_{0.5eV}^{20MeV} \frac{\sigma_\gamma(E)}{E} dE \tag{4}$$

This makes the assumption that the flux has a 1/E spectrum. In order to calculate the resonance integral an ENDF file was created with the new resonance parameters. Then, using the nuclear data processing code NJOY [7], a Doppler-broadened (298K) PENDF file was created and input to the code INTER [8] which will perform the calculation of the resonance integrals. To obtain the uncertainty in the RI_γ this process was repeated many times using a Monte Carlo method to perturb the neutron widths, capture widths, and resonance energies along a Gaussian distribution with standard deviation equivalent to the uncertainties on the final parameters listed in Table 1 (arbitrarily small uncertainties for unvaried ENDF/B-VII.1 values). This process has been used in propagation of uncertainties in nuclear reactor calculations for constants such as the neutron effective multiplication factor k_{eff} [9], and in calculations of the RI_γ in previous publications [10]. The final calculated RI_γ from this method is 0.07% different from an INTER calculated capture resonance integral of ENDF/B-VII.1 values. If the RI_γ is calculated between 2 keV and 20 MeV, the RPI value is 4% less than ENDF/B-VII.1. These are the expected results because the strong low energy resonance dominating the RI_γ is unchanged in this evaluation, and higher energy resonances have increased neutron widths. The strength function S_0 was calculated from Eq. 5, where ΔE is equivalent to the energy range over which the strength function was calculated and where the angular momentum quantum number l=0 [11].

$$S_l = \frac{1}{(2l+1)\Delta E} \sum_j \Gamma_{nj}^l \tag{5}$$

The values of Γ_{nj}^l are the reduced neutron widths for a given l, which is given by Eq. 6, where Γ_{nj} are the measured values of neutron widths for each resonance, E_0 is the energy at which the resonance occurs, and V_l is the penetrability factor for a square potential well.

$$\Gamma_{nj}^{l} = \sqrt{\frac{1eV}{E_0}}\frac{\Gamma_{nj}}{V_l} \tag{6}$$

In the case of s-wave neutrons, however, V_l is simply equal to one. Although the resonance parameter analysis was performed for the energy region of 0.113-20 keV, to avoid inclusion of missing levels the strength function S_0 was calculated using the s-wave contributions in the energy region of 0.131-12 keV. Complications such as multiple isotopes in a sample, multiple spin states in an isotope, or overlap of strong and weak resonances may cause resonance levels to be missed. To identify whether levels may have been missed, Dyson and Mehta developed a statistical test Δ_3 [12] that provides a measure of the deviation of observed energy levels and the deviation of theoretical energy levels. This test is contained in the distribution of SAMMY 8.0, and is shown in the SAMDIST manual [13]. To determine a region in which levels would not likely be missed, a comparison of observed and theoretical Δ_3 values was employed. The observed number of resonances departs from theory at approximately 12 keV. The cumulative levels and average level spacing are plotted in Figure 5 illustrating the departure from theory and selection of energy region.

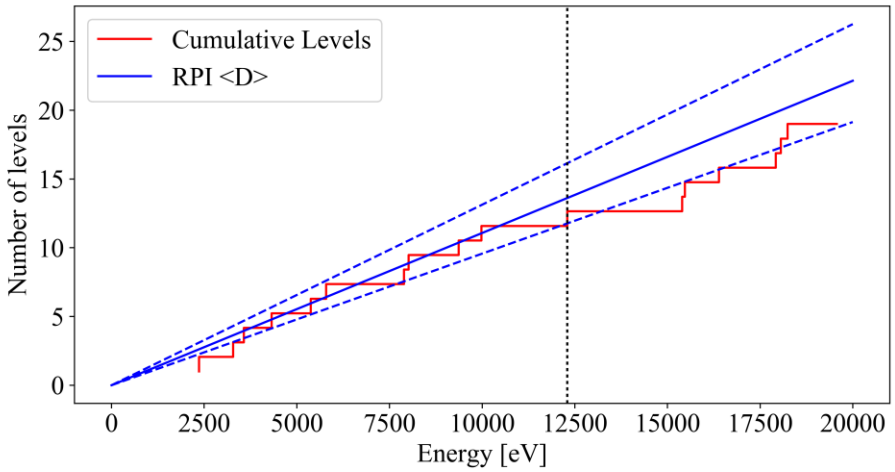

Figure 5. Cumulative levels in ^{96}Mo and the corresponding linear fit with error given by the Wigner probability distribution as described in Ref. 9. The vertical line shows the cutoff for the strength function as determined by the Δ3 analysis.

This energy region leaves 12 energy levels to sum reduced neutron widths, which was an adequate sample size to use similar methods as described in Ref. 11. The uncertainty of the strength function σ_{S_0} given in Eq. 9 is the quadrature sum of the propagated variance from the experimental uncertainties given by Eq. 7, and the variance of the Porter Thomas distribution given in Eq. 8.

$$\sigma_{exp}^2(\Gamma_{n,i}) = \left(\sum_i \sum_j \frac{\partial S(\Gamma_{n,i})}{\partial \Gamma_{n,i}} \frac{\partial(\Gamma_{n,j})}{\partial \Gamma_{n,j}} cov(\Gamma_{n,i}, \Gamma_{n,j})\right) \tag{7}$$

$$\sigma_{PT}^2(S_0) = \frac{2}{N} S_0^2 \tag{8}$$

$$\sigma_{S_0} = \sqrt{\sigma_{exp}^2(\Gamma_{n,i}) + \sigma_{PT}^2(S_0)} \quad (9)$$

Using Eq. 5 and 9 to calculate the s-wave strength function results in $S_0 = 0.82 \pm 0.32$. The uncertainty is dominated by the variance of the Porter Thomas distribution, which is bound by the number of resonances participating in the calculation. S_0 calculated from the Atlas of Neutron Resonances [11] neutron widths in this same energy region 0.51 ± 0.25 is smaller by ~40% compared to the RPI S_0. This increase in the S_0 is due to increased neutron widths in the 1-4 keV energy region resulting from the RPI analysis.

6. CONCLUSIONS

New parameters have been fitted for the isotope ^{96}Mo, improving neutron widths, J^{π}, and energy values from the previous ENDF/B-VII.1 evaluation. These new resonance parameters resulted in a strength function of 0.82 ± 0.32 as compared to 0.63 ± 0.30 stated in the Atlas by Brookhaven National Laboratory (BNL), and have an unchanged capture resonance integral as compared to ENDF/B-VII.1 and the BNL value of 17 ± 3 b. The increase in the s-wave strength function and reduction of capture resonance integral above 2 keV are both a result of the slight increases in neutron widths that were obtained from this analysis.

ACKNOWLEDGMENTS

We thank the LINAC technicians who operate the accelerator and provide mechanical and electronic assistance.

REFERENCES

1. R. Bahran, *A New High Energy Resolution Neutron Transmission Detector at the Gaerttner LINAC Center and Isotopic Molybdenum total Cross Section Measurements in the keV-Region,* RPI Ph.D. Dissertation, 2013
2. R. Bahran et al., "Isotopic molybdenum total neutron cross section in the unresolved resonance region," *Physical Review C*, **92**(2), (2015).
3. Y. Danon, et. al., "Nucl. data for criticality safety and reactor applicat. at the Gaerttner LINAC Center," *Ameri. Nucl. Soc. Winter Meeting,* San Diego, CA, 2012.
4. G. Knoll, *Radiation Detection and Measurement,* Ch. 8, John Wiley & Sons Inc.,USA (2010)
5. R. Bahran, et. al., *10th Int. Topical Meeting Nucl. Applicat. of Accelerators, AccApp'11*, Knoxville TN
6. A. Youmans, et. al., "Using Simulations To Determine The Energy Resolution Function Of Neutron Time-Of-Flight Experiments", *Transactions of the American Nuclear Society*, vol. 109, p. 861, 2014.
7. R.E. McFarlane et al., *NJOY99.0*, Los Alamos National Laboratory, New Mexico (1999).
8. C.L. Dunford, "ENDF Utility Codes Release 6.12," Informal Report (2001)
9. D. Rochman, W. Zwermann et al, "Efficient use of Monte Carlo: Uncertainty Propagation," *Nucl. Sci. Eng.*, **177**, 337 (2014).
10. R.C. Block, et. al., "Neutron transmission and capture measurements and analysis of Dy from 0.01 to 550 eV", *Prog. Nucl. Energy,* **94**, pp.126-132, (2017)
11. S.F. Mughabghab, *Atlas of Neutron Resonances*, Elsevier, Oxford, UK, p. 23 (2006) .
12. F.J. Dyson, ML Mehta, "Statistical Theory of the Energy Levels of Complex Systems," *Journal of Mathematical Physics 4*, **5**, (1963), pp. 701-712.
13. L.C. Leal, N.M. Larson, *SAMDIST: A Computer Code for Calculating Statistical Distributions for R-Matrix Resonance Parameters*, Oak Ridge National Laboratory, Oak Ridge, Tennesssee, p. 4 (1995).